

## Three-dimensional CFD Study of Free-Surface Flow in a Sharply Curved 30° Open-Channel Bend

Omid Seyedashraf<sup>1,\*</sup> and Ali Akbar Akhtari<sup>2</sup>

<sup>1</sup>Department of Civil Engineering, Kermanshah University of Technology, Kermanshah, Iran.

<sup>2</sup>Department of Civil Engineering, Razi University, Kermanshah, Iran.

Received 16 December 2016; Accepted 20 January 2017

### Abstract

In this study, the air-water two-phase flow in a strongly curved 30° open-channel bend is numerically simulated and analyzed. The research is motivated by the fact that most of the sharp or mild bend flow studies are focused on the 90, 120, and 180° bends. Although these curvatures form from the bends with lower degrees, i.e. 30° curvatures, there is no published work in this field. Due to the paucity of data in the literature, the CFD procedure here is validated using the experimental data of a sharp 90° bend of a previous study. The Reynolds-averaged Navier–Stokes equation system is used as the governing equations and the finite volume method is employed for the discretizations. The Volume of Fluid free-surface tracking method, in conjunction with the Standard k-ε turbulence model, is utilized for the air-water interactions and turbulence closure. It is found that the secondary flow intensity in the 30° bend is minor than the 90° bends. However, the tendency to flow separation is more intense in these bends, which is due to the momentum of the fluid particles passing the curvature. The results of this study may be used to control the river morphology.

*Keywords:* flow separation; open channel bend; converging bends; turbulence modeling.

### 1. Introduction

Natural waterways do not remain straight [1]. Accordingly, finding a river remaining straight for a length near to a tenth of its width is very rare. River bends are the self-induced plan deformation of the waterway caused by the three-dimensional nature of the flow [2]. Considering the shape of curvatures, strongly curved open-channels are obtained when  $R/b < 3$ , where  $R$  is the radius of the bend and  $b$  is the width of the flume [3]. The increase of this ratio increases the flow turbulence [4].

When the fluid particles enter the beginning of the bend, a secondary flow forms in the cross-section of the channel. This is because of the fluctuations between the pressure gradients and centrifugal forces of the fluid particles. The phenomenon is the most significant features of the curved flows and includes the helical streamlines along the curvatures. This flow changes the erosion and sedimentation pattern in rivers and their morphology by increasing the degree of the meanderings. Consequently, predicting the bend shape changes may be important to analyze the secondary flow intensity and reduce the bank erosion and sedimentation.

Strongly curved open-channels, especially the sharp 30° bends are regularly seen in rivers. Due to the three-dimensional and complex nature of these flows, the experimental and numerical investigation of the topic has fascinated researchers for the past decades. Many investigations have been conducted including the 90, 120,

and 180° bends [5-9]. For example, Blanckaert and De Vriend [9] measured the turbulent stress components of curved currents and analyzed the flow turbulence in a sharp 120° bend. Seyedashraf and Akhtari [10] investigated the flow features in a strongly curved 90° channel and addressed a new method to minimize the flow separation after the bend. Vaghefi, Safarpour [8] analyzed the effect of sediment density on the bed topography both in the mild and in the sharp 90° bends considering a T-shaped spur dike at the middle of the outer bank by the SSIM code. However, no work has been reported neither for the mild nor sharp bends with lower-degrees, e.g. 30° bends, which are the antecedent shape of the previously investigated bends.

In this study, the experimental results of Akhtari, Abrishami [11]'s investigations on the flow pattern in a sharply curved 90° open-channel is used to validate a new numerical simulation of a sharp 30° bend. Two numerical simulations are carried out, namely a 90° bend for the validation process, and a 30° bend model as the main objective of the work. The rest of this paper is organized as follows. In Section 2, the model apparatus is described. Section 3 presents the numerical procedures for the CFD simulations. The results are given in Section 4. Finally, in Section 5 the findings of the study are summarized.

### 2. Model geometry

In this study, Akhtari [12]'s laboratory flume was numerically simulated. The model consists of a strongly curved 90° bend attaching two straight open-channels. In the validation case, the numerical results were compared with the experiments conducted at the Ferdowsi University of Mashhad. After the validation process, the same exact CFD

\*E-mail address: o.seyedashraf@kut.ac.ir.

ISSN: 1791-2377 © 2017 Eastern Macedonia and Thrace Institute of Technology. All rights reserved.

doi:10.25103/jestr.103.12

configurations will be used to simulate a similar flume with a sharp 30° bend, which has not been studied before. The latter flume case is a 0.40×0.40m<sup>2</sup> rectangular flume, which comprises a straight 3.60m long channel, a sharp 30° bend, and a straight 1.80m channel. The system connects a head tank to a downstream tank (Figure 1). The channel is made of Plexiglas, thus, the roughness parameter is ignored in the CFD process.

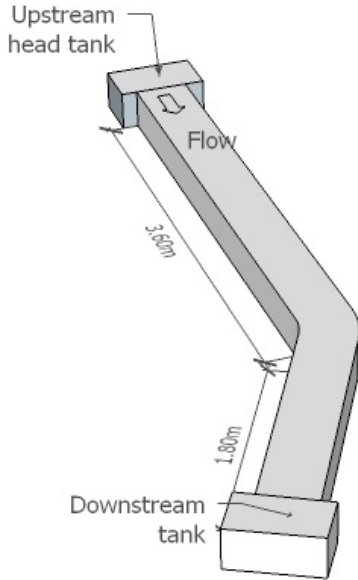


Fig. 1. The model geometry of the 30° bend case.

### 3. Numerical simulation

#### 3.1. Governing equations

The Reynolds-Averaged Navier-Stokes (RANS) equation system was adopted as the governing equations in this study. The system is based on the conservation of mass, momentum, and energy. The finite volume model (FVM) was adopted to conduct the numerical computations. Here, the FVM involves the discretization and integration of the RANS equations over the computational cells of the flow region. In this study, since water is assumed to be incompressible and the heat transfer does not affect the flow mechanism, the energy equation was disregarded from the system. Accordingly, the RANS system in its generalized Cartesian coordinates (x, y, z) form was considered as follows:

$$\frac{\partial(\rho)}{\partial t} + \frac{\partial(\rho u_i)}{\partial x_i} = S_m, \quad (1)$$

$$\frac{\partial(\rho u_i)}{\partial t} + \frac{\partial(\rho u_i u_j)}{\partial x_j} = -\frac{\partial p}{\partial x_i} + \frac{\partial}{\partial x_j} \mu \left[ \frac{\partial u_i}{\partial x_j} + \frac{\partial u_j}{\partial x_i} \right] + \frac{\partial(-\rho \overline{u_i' u_j'})}{\partial x_j}, \quad (2)$$

in which t is time, u<sub>i</sub> is the i<sup>th</sup> component of the Reynolds-averaged-velocity, x<sub>i</sub> the i<sup>th</sup> axis of the coordinate system, ρ is the water density, p is the Reynolds averaged pressure, g is the gravity acceleration, μ is the viscosity, and S<sub>m</sub> is the mass exchange between water and air. The term (-ρ*u<sub>i</sub>'u<sub>j</sub>'*) denotes the Reynolds-stress parameter, which has to be resolved to close the momentum equations. The Boussinesq theory was adopted to do this, which correlates the Reynolds-Stresses to the mean rate of deformation:

$$-\rho \overline{u_i' u_j'} = \mu_t \left( \frac{\partial u_i}{\partial x_j} + \frac{\partial u_j}{\partial x_i} \right), \quad (3)$$

where μ<sub>t</sub> is the turbulent viscosity.

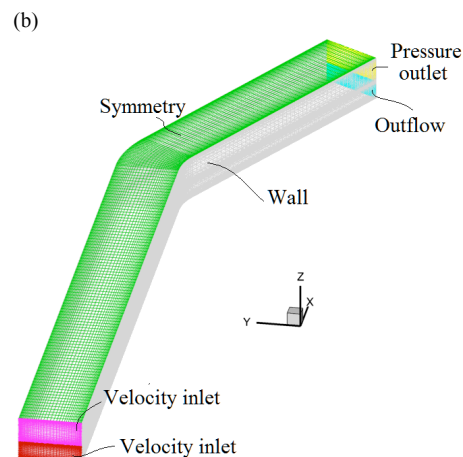
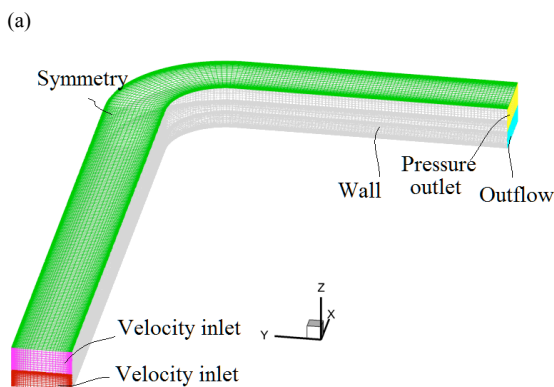
#### 3.2. Grid form and boundary conditions

The computational domain was discretized into 372,000 hexahedral control volumes divided by 1,098,100 quadrilateral interior faces and 390,156 nodes. The grid was refined near the regions with important effects on the flow characteristic, i.e. the channel walls, bottom, and the air-water interaction surface. The velocity inlet, outflow, wall, and pressure outlet were employed as the working boundary conditions, which are summarized in Table 1.

Figure 2 illustrates the meshing form and the employed boundary conditions.

Table 1. Boundary conditions.

Boundary	Boundary conditions	Specifications
Water inlet	Velocity inlet	0.394 m/s
Air inlet	Velocity inlet	1e-07 m/s
Water outlet	Outflow	Flow weight=1
Air outlet	Pressure outlet	---
Channel bank	Wall	No roughness
Channel bottom	Wall	No roughness



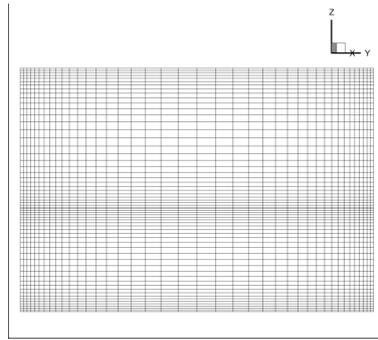


Fig. 2. The meshing form and boundary conditions: (a) 90° bend case, (b) 30° bend case, (c) section view of the grid form for both models.

### 3.3. Numerical procedure

The overall employed CFD procedure is as follows:

- The Pressure-Implicit with Splitting of Operators (PISO) model was used for the velocity-pressure couplings, which is a non-iterative method [13].
- The Pressure Staggering Option (PRESTO) algorithm was applied to the models to deal with the pressure discretization. This model is suitable for the swirling flows [14].
- The Second Order Upwind model was used to deal with the momentum and turbulence equations [15].
  - The modified HRIC model was adopted for the volume fraction computations [16].
  - Finally, the Volume of Fluid (VOF) free surface model was used to resolve the air-water interactions. The model is formulated based on the fact that two or more fluid zones do not interpenetrate. Moreover, the volume fractions of both zones sum to unity in the computational cell [17].

About 3,258 iterations were conducted to achieve convergence. The important hydraulic and numerical parameters are summarized in Table 2.

Table 2. Hydraulic parameters, and numerical specifications.

Turbulent kinetic	Turbulent dissipation	Mean velocity	Reynolds number
5.39E-2	5.48E-2	39.40	36765

### 3.4. Turbulence model

The Standard k-ε model in conjunction with the non-equilibrium wall-function treatment was used to resolve the turbulent structure of the water flow. The necessary features of the adopted model are presented in this subsection, however, the readers may refer to [10, 18]. The mathematical formulation of this model relies on the transport equations for the kinetic energy (k) and the dissipation rate (ε). These oscillation terms may be linked to the flow momentum by the Boussinesq hypothesis:

$$\frac{\partial(\rho k)}{\partial t} + \text{div}(\rho k \mathbf{U}) = \text{div} \left[ \frac{\mu_t}{\sigma_k} \text{grad } k \right] + 2\mu_t E_{ij} \cdot E_{ij} - \rho \epsilon, \quad (4)$$

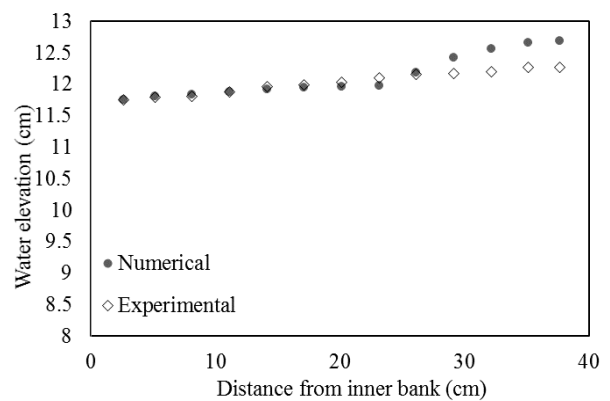
$$\frac{\partial(\rho \epsilon)}{\partial t} + \text{div}(\rho \epsilon \mathbf{U}) = \text{div} \left[ \frac{\mu_t}{\sigma_\epsilon} \text{grad } \epsilon \right] + C_{1\epsilon} \frac{\epsilon}{k} 2\mu_t E_{ij} \cdot E_{ij} - C_{2\epsilon} \rho \frac{\epsilon^2}{k}, \quad (6)$$

in which  $\mathbf{U}$  is the velocity matrix,  $E_{ij}$  is the mean rate of deformation tensor.  $C_{1\epsilon}$  and  $C_{2\epsilon}$  are constants with the 1.44 and 1.92 values, respectively.  $\sigma_k = 1$  and  $\sigma_\epsilon = 1.3$  are the Prandtl numbers, which relate the diffusivities of  $k$  and  $\epsilon$  to the eddy viscosity.

### 4. Model validation

To obtain reliable results, the numerical model was first validated by comparing its results with the existing experimental data. Accordingly, the experimental model of a previous study was numerically simulated. The same procedure was then used to extend the work to the new 30° open-channel bend, which has not been addressed in the literature.

Figures 3 and 4 compare the measured and simulated water depth and velocity changes. The velocity values were calculated considering the  $x$ ,  $y$ , and  $z$  component ( $\sqrt{u^2 + v^2 + w^2}$ ). It can be seen that the numerical model has accurately captured the main features of the flow in the 90° bend. As previously mentioned, the fluid particles move in a helical path when water reaches the beginning of the bend. This alters the water surface balance and causes super-elevation throughout the bend and after it. The phenomenon makes velocity fluctuate. In sharp 90° bend cases, the phenomenon induces the flow separation after the bend. The velocity and water depth values are increased and reduced near the inner (concave) and outer (convex) banks of the bend, respectively.



(a)

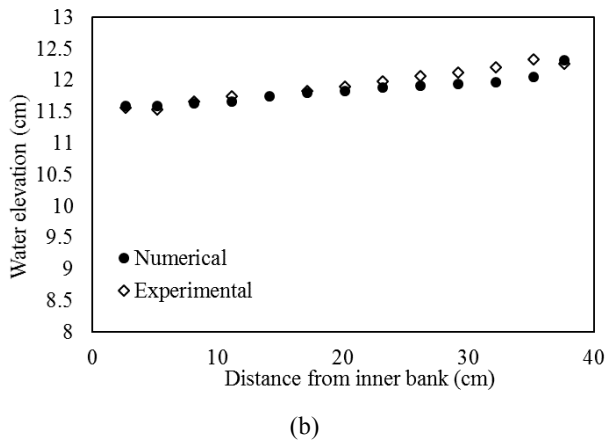


Fig. 3. Experimental and numerical water depth results; (a) 0° section; (b) 90° section [11].

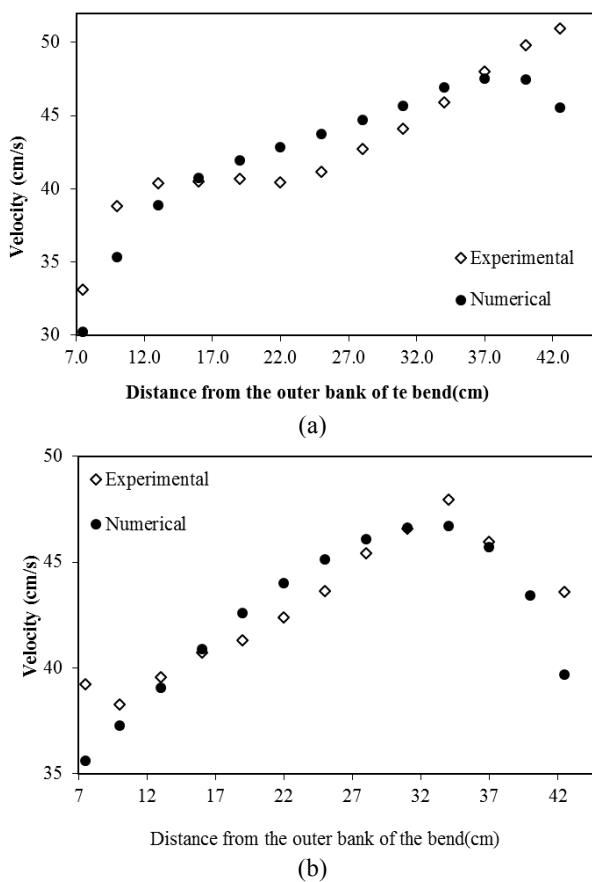


Fig. 4. Experimental and numerical velocity results; (a) 0° section; (b) 90° section.

The root mean square error (RMSE) of the obtained data was calculated to measure the accuracy of the numerical simulations.

$$RMSE = \left[ \frac{\sum_{i=1}^N (X_i(Exp) - X_i(Pred))^2}{N} \right]^{0.5} \quad (7)$$

in which  $N = 13$  is the number of measured data, where ‘ $X(Exp)$ ’ and ‘ $X(Pred)$ ’ are the measured and predicted values, respectively.

Table 3 summarizes the obtained RMSEs of the 90° bend model.

Table 3. RMSEs of the 90° bend model.

0°	45°	90°	40(cm)	80(cm)
5.80	6.56	9.45	4.40	5.60

Figures 5 and 6 depict the velocity contours and the streamwise/tangential velocity vectors of the both models. The figures clearly show the maximum and minimum values of the flow rate in the bend.

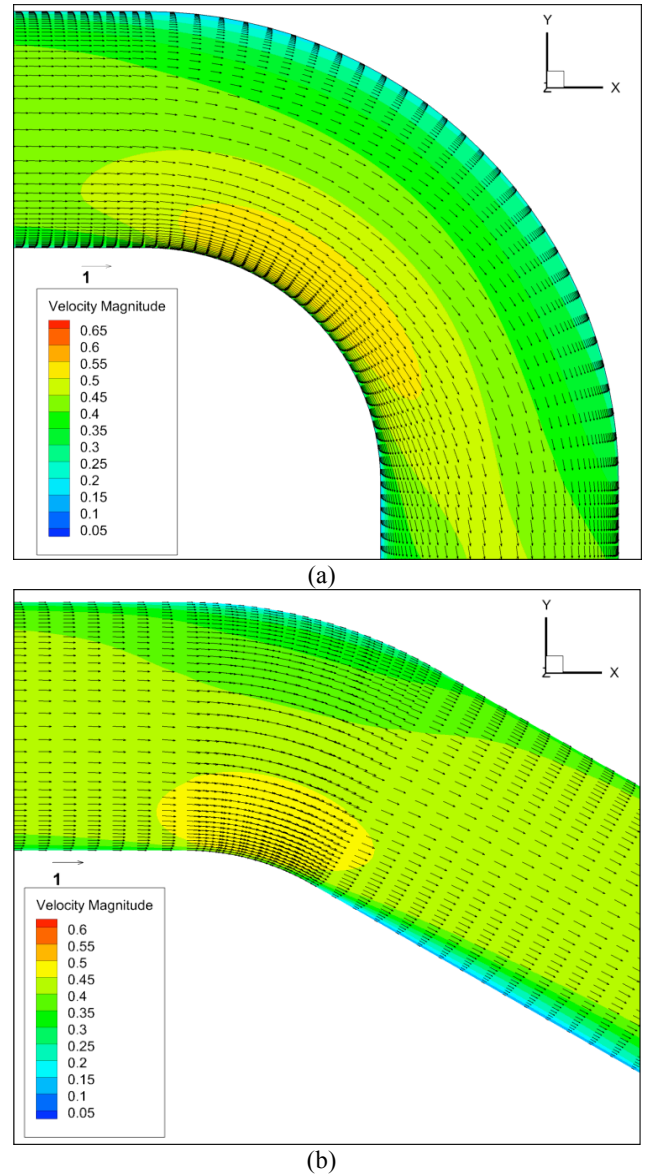


Fig. 5. Velocity contours and vectors of the numerical simulations in the curved section; (a) 90° bend case, (b) 30° bend case.

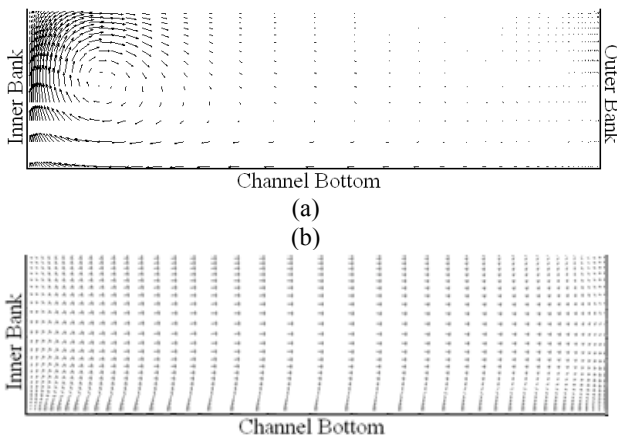


Fig. 6. Secondary flow at the end of the curvature; (a) 90° bend model, (b) 30° bend model.

It can be seen that the flow velocity is reduced near the convex walls in both cases. The helical motion of the flow shifts the maximum velocity near the concave bank of the curvature, and the minimum flow rate to the outer bank. This, especially in the 90° case, causes water surface level gradients, which is noticeable by the blue contour color about the convex wall. On the other hand, it can be acknowledged that, in the 30° bend model, the probability of flow separation is stronger than the 90° test case although the secondary flow in the 30° bend case is very weak (Figure 6). In this case, the tendency to flow separation is because of the flow momentum.

## 5. Conclusions

This study has examined the flow behavior in the sharp 30° open-channel bends through CFD simulations. The main results of this work can be summarized as follows:

- The intensity of the helical motion of fluid particles in sharp bends depends on the shape of the bend. The observed strong secondary current at the end of the sharp 90° bend was not seen in the 30° test case examined here.
- The helical flow makes the water depth decrease, while increasing the flow rate, near the concave banks of the bend in the both 90 and 30° bend cases.
- According to the tangential velocity vectors, the fluid particles move toward the inner bank of the bend from about the channel bottom and then shift toward the outer bank after reaching the free surface. This happens in the 90° bends more quickly in comparing with the 30° bend models.
- Although the secondary flow was not intense in the 30° bend model, the tendency to flow separation was noticeable after the curvature.
- The employed numerical model, compromising the VOF free surface model and Standard k- $\epsilon$  turbulence model, was able to capture the main features of the helical flow in the sharp open-channel bends.

This is an Open Access article distributed under the terms of the Creative Commons Attribution Licence



## References

1. Leopold, L.B. and M.G. Wolman, *River meanders*. Geological Society of America Bulletin, 1960. **71**(6): p. 769-793.
2. Yalin, M.S., *River mechanics*. 2013: Elsevier.
3. Leschziner, M.A. and W. Rodi, *Calculation of strongly curved open channel flow*. Journal of the Hydraulics Division, 1979. **105**(10): p. 1297-1314.
4. Ottevanger, W., K. Blanckaert, and W. Uijttewaal, *Processes governing the flow redistribution in sharp river bends*. *Geomorphology*, 2012. **163**: p. 45-55.
5. Farhadi, A., et al. *Experiments on two consecutive open channel bends*. in *7th International Conference on Fluvial Hydraulics, RIVER FLOW 2014*. 2014. Lausanne: CRC Press/Balkema.
6. Ghobadian, R. and K. Mohammadi, *Simulation of subcritical flow pattern in 180° uniform and convergent open-channel bends using SSIM 3-D model*. *Water Science and Engineering*, 2011. **4**(3): p. 270-283.
7. Vaghefi, M., M. Akbari, and A. Fiouz, *An experimental study of mean and turbulent flow in a 180 degree sharp open channel bend: Secondary flow and bed shear stress*. *KSCE Journal of Civil Engineering*, 2015: p. 1-12.
8. Vaghefi, M., Y. Safarpour, and S.S. Hashemi, *Effect of Sediment Density on the Bed Topography in a Channel Bend Using Numerical Modeling* *The Journal of Engineering Research*, 2016. **13**(1).
9. Blanckaert, K. and H. De Vriend, *Turbulence characteristics in sharp open-channel bends*. *Physics of Fluids (1994-present)*, 2005. **17**(5): p. 055102.
10. Seyedashraf, O. and A.A. Akhtari, *Flow separation control in open-channel bends*. *Journal of the Chinese Institute of Engineers*, 2016. **39**(1): p. 40-48.
11. Akhtari, A., J. Abrishami, and M. Sharifi, *Experimental Investigations Water Surface Characteristics in Strongly-Curved Open Channels*. *Journal of Applied Sciences*, 2009. **9**(20): p. 3699-3706.
12. Akhtari, A.A., *Surveying flow in strongly-curved open channel and evaluation of the effect of internal non submerged vanes on flow pattern through the bends*, in *Civil Engineering*. 2010, Ferdowsi University of Mashhad.
13. Jang, D., R. Jetli, and S. Acharya, *Comparison of the PISO, SIMPLER, and SIMPLEC algorithms for the treatment of the pressure-velocity coupling in steady flow problems*. *Numerical Heat Transfer, Part A: Applications*, 1986. **10**(3): p. 209-228.
14. Dutta, T., K. Sinhamahapatra, and S. Bandyopdhyay, *Comparison of different turbulence models in predicting the temperature separation in a Ranque-Hilsch vortex tube*. *International Journal of Refrigeration*, 2010. **33**(4): p. 783-792.
15. Warming, R. and R.M. Beam, *Upwind second-order difference schemes and applications in aerodynamic flows*. *AIAA Journal*, 1976. **14**(9): p. 1241-1249.
16. Muzaferija, S., et al. *A two-fluid Navier-Stokes solver to simulate water entry*. in *Proceedings of the 22nd symposium on naval hydrodynamics, Washington, DC*. 1998.
17. Hirt, C.W. and B.D. Nichols, *Volume of fluid (VOF) method for the dynamics of free boundaries*. *Journal of computational physics*, 1981. **39**(1): p. 201-225.
18. Seyedashraf, O. and A. Akhtari, *Evaluation of Various Turbulence Models in Predicting Flow Behaviours in Meandering Channels*, in *9th International River Engineering Conference 2013*: Shahid Chamran University.